Landau level structures and semimetal-semiconductor transition in strained InAs/GaSb quantum wells

A. Zakharova
Institute of Physics and Technology of the Russian Academy of Sciences, Nakhimovskii Avenue 34, Moscow 117218, Russia

S. T. Yen
Department of Electronics Engineering, National Chiao Tung University, Hsinchu, Taiwan, Republic of China

K. A. Chao
Department of Physics, Lund University, Sölvegutun 14A, S 233 62 Lund, Sweden
(Received 30 January 2003; revised manuscript received 12 June 2003; published 17 March 2004)

Using Burt's envelope function theory and the scattering matrix method, we investigate the hybridized electron-hole Landau levels in strained InAs/GaSb quantum wells sandwiched between wide-gap AlSb barrier layers under electric and a quantizing magnetic fields applied perpendicular to interfaces. At zero magnetic field, in the structures studied here, the lowest electron level in the InAs layer lies below the highest heavy-hole level in the GaSb layer. With increasing magnetic field, the electron levels move up and the heavy-hole levels move down, producing anticrossings and gaps in the Landau level structures. We have found that the Landau level structures depend strongly on the lattice-mismatched strain and the applied voltage. As a result, in the region before anticrossings, the g factor of the lowest electron Landau level has a larger value for the quantum well structure grown on GaSb than that for the structure grown on InAs, while in the region after anticrossings the situation reverses for the g factor. Under low magnetic field, the difference between the electron g factors for the structures grown on different substrates is found to be as large as 10 for zero bias and decreases significantly with increasing bias. When all electron levels become higher than hole levels at high magnetic fields, the semimetal-semiconductor transition occurs. The critical magnetic field B_c for the phase transition in structures grown on InAs is found to be lower than that in structures grown on GaSb. It is also obtained that a positive voltage biased across the InAs/GaSb well essentially decreases B_c. Therefore, for a fixed magnetic field, the semimetal-semiconductor transition can be controlled by a bias.

DOI: 10.1103/PhysRevB.69.115319 PACS number(s): 73.21.Ac, 73.21.Fg

I. INTRODUCTION

The semimetal-semiconductor phase transition (SSPT) in InAs/GaSb/AlSb heterostructures has been a subject of investigations for more than 20 years.[1–21] Going from the semimetal phase to the semiconducting phase, the bipolar conductivity of InAs/GaSb superlattices and InAs/GaSb/AlSb quantum wells changes to a unipolar electron conductivity. Such an SSPT was studied in the InAs/GaSb superlattices with decreasing period.[1–3,5,7,18,20] The SSPT was also observed experimentally and studied theoretically under high magnetic fields,[4,6,8,9,12–14,16,18] as well as in InAs/$Al_xGa_{1-x}Sb$ quantum wells with an increasing Al concentration.[8,15,17] The observation of the SSPT in InAs/GaSb superlattices under hydrostatic pressure was also reported.[10] The lattice-mismatched strain can also induce a SSPTs in InAs/GaSb quantum well structures.[21] In the present paper, we investigate the Landau level structures in strained InAs/GaSb quantum wells sandwiched between two AlSb barrier layers, and the SSPT under the influence of a bias across the structures and/or a magnetic field perpendicular to the interfaces.

In a broken-gap AlSb/InAs/GaSb/AlSb quantum well, the InAs conduction band overlaps with the GaSb valence band, as shown in Fig. 1. If the lowest quantized electron level in the InAs conduction band lies below the highest hole quantized level in the GaSb valence band, the electrons from the GaSb valence band can move to the InAs conduction band, producing a positive hole charge in the GaSb layer and a negative electron charge in the InAs layer. In this case the parallel transport of both electron gas and hole gas contributes to the current in the InAs/GaSb well when an external bias is applied parallel to interfaces. This is a semimetal phase. An external magnetic field shifts down the hole levels in the GaSb layer and shifts up the electron levels in the InAs layer, eventually driving the electrons from the InAs conduc-

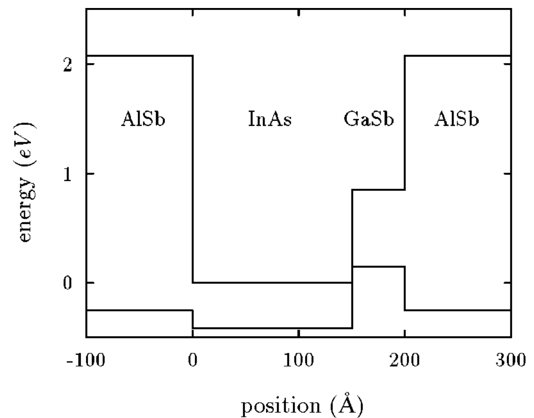

FIG. 1. Conduction and valence band diagram of the AlSb/InAs/GaSb/AlSb quantum well structure with a 15-nm InAs layer and a 5-nm GaSb layer.

 ©2004 The American Physical Society

tion band back to the GaSb valence band. The system is then in a semiconducting phase and exhibits a unipolar electron conductivity with an electron concentration much less than that in the semimetal phase.

The Landau level structures and the SSPT in InAs/GaSb superlattices under a magnetic field applied perpendicular to interfaces have been studied theoretically in Refs. 6 and 9, using the flatband approximation. The same approximation has also been used to investigate the Landau level structures in InAs/AlGaSb quantum wells.[15] In the present paper, we will show that the SSPT can be induced by a magnetic field and an electric field both applied perpendicular to the interfaces. We will calculate the Landau level structures in InAs/GaSb quantum wells, using the Burt envelope function theory[22] and its application to zinc-blende structures developed by Foreman.[23] The scattering matrix method,[24] as described in Ref. 25, will be employed to obtain the energy levels in structures with thick InAs layers. In these structures, in the absence of external magnetic and electric fields, the lowest electron quantized level is lower than the highest hole quantized level at zero in-plane wave vector. Recently, such quantum wells have been investigated experimentally.[12,16,26,27] In these quantum wells and similar superlattices, anticrossings of electron and hole subbands at nonzero in-plane wave vectors cause strong hybridizations of the electron and hole states[5,7,11–16,18–21,25–31] accompanied by the appearance of gaps in the in-plane dispersions. Then, near the highest gap conduction-band-like and valence-band-like subbands are formed with positive and negative effective masses, respectively. This can result in a semiconducting behavior in spite of the formation of a negative charge in the InAs layer and a positive charge in the GaSb layer. The situation changes when a magnetic field is applied, and the states are characterized by a quantum number n. In this case, only the states with the same quantum number n interact, and hence similar anticrossings and gaps have been found in the Landau level structures of InAs/GaSb superlattices[6,9] and InAs/AlGaSb quantum wells.[15] However, the highest hole and lowest electron Landau levels have different quantum numbers and do not interact. They cross at some critical magnetic field B_c at which no strong hybridization of the electron and hole levels exists. Then the SSPT occurs. The behavior of the system at the intermediate magnetic fields ($0<B\ll B_c$) is still unclear. Hence, a detailed investigation is necessary to identify the magnetotransport processes.

An important feature in the present paper, as compared to previous works, is the consideration of the lattice-mismatch strain effect on the hybridized electron-hole Landau level structures in broken-gap heterostructures. The strain comes from the lattice mismatch between the InAs/GaSb quantum well and the InAs substrate or the GaSb substrate. It is found that the energy level positions in the considered structures and spin splittings of the levels are sensitive to which substrate the quantum well is grown on. The use of Burt's theory for the investigation of the Landau level structures is also an aspect of the present work. We believe that because of this, for both sample structures, interesting results are obtained here which are qualitatively different from those in Ref. 15. For example, we have found a strong enhancement of the spin splitting of the lowest electronlike Landau levels after anticrossings with the holelike states, and this spin splitting is much larger than that of the highest holelike Landau levels at high magnetic fields. We also found that the critical magnetic field, at which the SSPT occurs, depends on substrate materials. Furthermore, because the normal electric field reduces the overlap between the InAs conduction band and the GaSb valence band, this critical field decreases with increasing positive bias voltage applied across the InAs/GaSb quantum wells. As a result, the electronlike and holelike states approach each other.[29] Consequently, at a given magnetic field, a semimetal phase will change to a semiconducting phase when the electric field increases. In the present paper, we describe our theoretical model in Sec. II, and the method of calculation in Sec. III. The results and a discussion are given in Sec IV.

II. THEORETICAL MODEL

To investigate the peculiarities of the Landau level structures in InAs/GaSb quantum wells, we add the strain Hamiltonian[32] to the six-band model described in Ref. 33, which takes into account the electron, light-hole, and heavy-hole states. We suppose that the structures are grown along [001] direction, which will be regarded as the z axis. We take the x axis to be along [100] and the y axis to be along [010]. Then the resulting total 6×6 $\mathbf{k}\cdot\mathbf{p}$ Hamiltonian $\hat{H}$ can be expressed as

$$\hat{H}=\hat{H}_K+\hat{H}_Z+\hat{H}_\epsilon . \tag{1}$$

Here $\hat{H}_K$ depends on the canonical momentum operators $\hbar\hat{K}_l=-i\hbar\partial/\partial l+|e|A_l/c$ ($l=x$, y, and z), where A_l is the l component of the vector potential, e is the electronic charge, and c is the speed of light. $\hat{H}_Z$ is the Zeeman term and $\hat{H}_\epsilon$ is the strain Hamiltonian. The matrices $\hat{H}_K$ and $\hat{H}_Z$ are presented in Ref. 33. They include, as parameters, the spatial variations of the conduction and valence band edges $E_c(z)$ and $E_v(z)$, the magnetic field B normal to the interfaces, the interband momentum matrix element P, which is supposed to be a constant value for all layers, and the modified Luttinger parameters γ_1, γ_2, and γ_3. The Luttinger parameters are functions of z since they depend on the materials of the structure.

Since the off-diagonal terms of the strain tensor ϵ_{ij} are equal to zero and $\epsilon_{xx}=\epsilon_{yy}$,[34] the strain Hamiltonian is represented by a diagonal matrix with elements

$$\begin{aligned}\hat{H}_{\epsilon 11}&=\hat{H}_{\epsilon 44}=a_c\epsilon,\\ \hat{H}_{\epsilon 22}&=\hat{H}_{\epsilon 55}=(a_v-b/2)(\epsilon_{xx}+\epsilon_{yy})+(a_v+b)\epsilon_{zz}, \\ \hat{H}_{\epsilon 33}&=\hat{H}_{\epsilon 66}=(a_v+b/2)(\epsilon_{xx}+\epsilon_{yy})+(a_v-b)\epsilon_{zz}.\end{aligned} \tag{2}$$

Here $\epsilon=\epsilon_{xx}+\epsilon_{yy}+\epsilon_{zz}$, a_c, a_v, and b are the deformation potential constants, and the components of the strain tensor are[34] $\epsilon_{xx}=\epsilon_{yy}=(a_0-a)/a$, $\epsilon_{zz}=-2C_{12}\epsilon_{xx}/C_{11}$, where a_0 and a are the lattice constants of the substrate and layer materials, respectively, and C_{11} and C_{12} are the stiffness con-

stants. The Hamiltonian has been written using a set of basis functions in the same order as in Ref. 33: $|s_{1/2,1/2}\rangle$, $|p_{3/2,1/2}\rangle$, $|p_{3/2,3/2}\rangle$, $|s_{1/2,-1/2}\rangle$, $|p_{3/2,-1/2}\rangle$, and $|p_{3/2,-3/2}\rangle$. The dispersions and wave functions are then obtained using the eigenvalue equation $\hat{H}\psi=E\psi$, where $\psi=(\psi_1\psi_2\psi_3\psi_4\psi_5\psi_6)^T$ is the multicomponent envelope function.

Note that we neglect the split-off valence bands because the energy levels of hybridized electron-hole states are much higher than the edge of these bands. We also disregard the linear-in-k terms in the Hamiltonian, Kane's B parameter, the interband deformation potential resulting from the lack of inversion symmetry in bulk zinc-blende crystals, and the spin-orbit interaction terms in the strain Hamiltonian.[35,36] This is because the contributions of the related terms to the Hamiltonian are negligibly small.[32] The described model differs from those used previously for investigation of the Landau level structures by taking into account the proper order of canonical momentum operators and material parameters in $\hat{H}_K$ in accordance with Burt's envelope function theory. This is important even for bulk solutions, because the operators of canonical momentum do not mutually commute.

III. SOLUTION OF THE SCHRÖDINGER EQUATION

We obtain the solutions for the bulk dispersions and wave functions similarly to Ref. 33, but taking into account the difference between second and third Luttinger parameters and the lattice-mismatched strain. Also, the boundary conditions are formulated to match the wave functions at the interfaces. To exclude unphysical spurious solutions from the model,[23] we disregard quadratic-in-$\mathbf{k}$ terms in $\hat{H}_{K11}$ and $\hat{H}_{K44}$. Also, we neglect the terms $\hat{H}_{Z11}$ and $\hat{H}_{Z44}$ in $\hat{H}_Z$ as in Ref. 33. The vector potential is taken in the following form: $A_y=Bx$ and $A_x=A_z=0$. Then $\hat{K}_x=-i\partial/\partial x$, $\hat{K}_y=-i\partial/\partial y+|e|Bx/\hbar c$, and $\hat{K}_z=-i\partial/\partial z=\hat{k}_z$.

The conduction band envelopes, ψ_1 and ψ_4, can be expressed in terms of valence band envelopes similarly to Ref. 33 as

$$\psi_1=(E-E_c-a_c\epsilon)^{-1}(\sqrt{2}iP\hat{k}_z\psi_2/\sqrt{3}+P\hat{K}_+\psi_3+P\hat{K}_-\psi_5/\sqrt{3}), \tag{3}$$

$$\psi_4=(E-E_c-a_c\epsilon)^{-1}(\sqrt{2}iP\hat{k}_z\psi_5/\sqrt{3}+P\hat{K}_-\psi_6+P\hat{K}_+\psi_2/\sqrt{3}), \tag{4}$$

where $\hat{K}_\pm=\mp i(\hat{K}_x\pm i\hat{K}_y)/\sqrt{2}$. Accordingly, the 6×6 matrix equation for ψ can reduce to the 4×4 matrix equation with vector function $\mathbf{F}=(\psi_2\psi_3\psi_5\psi_6)^T$:

$$\hat{H}H_4\mathbf{F}=E\mathbf{F}. \tag{5}$$

The 4×4 Hamiltonian $\hat{H}_4$, which depends on the energy E, can be obtained from the Hamiltonian $\hat{H}$ by removing the rows and columns corresponding to the conduction band, and replacing γ_1, γ_2, and γ_3 with

$$\gamma_1'=\gamma_1-E_p[3(E-E_c-a_c\epsilon)]^{-1}, \tag{6a}$$

$$\gamma_{2,3}'=\gamma_{2,3}-E_p[6(E-E_c-a_c\epsilon)]^{-1}, \tag{6b}$$

where $E_p=2mP^2/\hbar^2$, and m is the free electron mass.

The boundary conditions for the vector functions $\mathbf{F}$ are formulated by integrating Eq. (5) across the interfaces of the abrupt heterojunctions.[22,23] As a result, the vector functions $\mathbf{F}$ and $\hat{H}_B\mathbf{F}$ are continuous at the interfaces, where $\hat{H}_B$ is a 4×4 matrix with nonzero elements: $\hat{H}_{B11}=\hat{H}_{B33}=GB$, $\hat{H}_{B22}=\hat{H}_{B44}=FB$, $\hat{H}_{B12}=SB_+$, $\hat{H}_{B34}=SB_-$, $\hat{H}_{B13}=TB_-$, $\hat{H}_{B31}=TB_+$, $\hat{H}_{B21}=CB_-$, and $\hat{H}_{B43}=CB_+$, where

$$GB=-\frac{\hbar^2}{2m}(2\gamma_2'+\gamma_1')\hat{k}_z,$$

$$FB=\frac{\hbar^2}{2m}(2\gamma_2'-\gamma_1')\hat{k}_z,$$

$$SB_\pm=\frac{\hbar^2}{m}\sqrt{6}i\gamma_3'\hat{K}_\pm+\frac{i\sqrt{2}}{\sqrt{3}}N_-\hat{K}_\pm, \tag{7}$$

$$CB_\pm=\frac{i\sqrt{2}}{\sqrt{3}}N_-\hat{K}_\pm,$$

$$TB_\pm=2i\sqrt{2}\left(\frac{\hbar^2}{2m}\gamma_3'+\frac{N_-}{3}\right)\hat{K}_\pm.$$

In Eq. (7), $N_-=-(\hbar^2/2m)(\gamma_1'-2\gamma_2'+1)$. Neglecting the warping terms in $\hat{H}_{K26}$, $\hat{H}_{K35}$, $\hat{H}_{K62}$, and $\hat{H}_{K53}$, which are proportional to $\gamma_2-\gamma_3$ as in Ref. 15, a solution for the envelope functions can be found in terms of a finite number of harmonic oscillator functions $f_\nu(x')$, where $f_\nu(x')=\exp(-qx'^2/2)H_\nu(\sqrt{q}x')$, for $\nu=0,1,2,\ldots$ $H_\nu(t)$ is the Hermite polynomial and $x'=x-x_0$ with $x_0=-k_y/q$, $q=|e|B/(\hbar c)$. $f_\nu(x')=0$ for $\nu<0$. The resulting multicomponent envelope function for each bulk state can be written in the following form:

$$\psi^{(n)}=\begin{pmatrix} C_1f_n(x') \\ C_2f_n(x') \\ C_3f_{n-1}(x') \\ C_4f_{n+1}(x') \\ C_5f_{n+1}(x') \\ C_6f_{n+2}(x') \end{pmatrix}\times\exp(ik_yy+ik_zz), \tag{8}$$

where the coefficients C_i determine the contribution of the corresponding Landau states to the total wave function. The values of k_z as well as the coefficients C_i, $i=1,2,\ldots,6$ for a given energy E are independent of x_0 and can be obtained similarly to Ref. 33. If $n=-2$, only one heavy-hole state with $\nu=n+2=0$ and spin $s=-1/2$ makes a contribution to wave function (8). For $n=-1$, the electron (light-hole) state of index $\nu=n+1=0$ and the heavy-hole state of index $\nu=n+2=1$ with spins opposite to the magnetic field direction are included in the solution. Five components enter the solution for $n=0$: two electron (light-hole) states of indices

$\nu=n=0$ and $\nu=n+1=1$ with spins along and opposite to the magnetic field direction and the heavy-hole state of index $\nu=n+2=2$ with spin $s=-1/2$. If $n\geqslant 1$, the contributions to the solution are from two electron (light-hole) states of indices n and $n+1$ with spins along and opposite to the magnetic field and two heavy-hole states of indices $n-1$ and $n+2$ with opposite spins.

We use the stepwise constant approximation for the potential distribution to obtain the solution of the Schrödinger equation employing the scattering matrix method, as described in Ref. 25. In each sublayer, the wave function is composed of all bulk states for a given quantum number n, energy E, and x_0. The boundary conditions are then used to match the wave functions at the interfaces between sublayers. In accordance with these boundary conditions, the mixing of the states at the interfaces occurs only for a given quantum number n so that we can solve the eigenvalue problem for each quantum number n one by one. If $n=-2$, only one heavy-hole state with spin $s=-1/2$ exists, and the scattering matrix is a 2×2 matrix. For $n=-1$, $n=0$, and $n\geqslant 1$ we have a 4×4, a 6×6, and 8×8 matrices because of the mixing at the interfaces of two, three, and four bulk states, respectively.[33] The employment of the scattering matrix algorithm, which has been shown to be more numerically stable than the conventional transfer matrix method, allows us to investigate the Landau level structures in thick InAs/GaSb broken-gap quantum wells. The details of calculation algorithm are presented in the Appendix.

IV. RESULTS AND DISCUSSION

To calculate the energy levels in the quantum wells under quantizing magnetic fields normal to the interfaces, from Ref. 30 we take parameters such as the energy gaps, the Luttinger parameters, the lattice constants, and the conduction and valence band offsets for the unstrained heterojunctions. The deformation potentials and the stiffness constants are taken from Ref. 37. The interband momentum matrix element P is obtained according to the InAs electron effective mass, which is $0.023m$. The quantum well structures grown on InAs and GaSb are considered. In the first case, the GaSb layer of the well is strained. Because of this, the edge of the heavy-hole valence band shifts upwards by 0.019 eV, and the edge of the light-hole band shifts downwards by 0.029 eV. In the quantum well structure grown on GaSb, the InAs layer of the well is strained and the conduction band edge shifts by -0.029 eV. The lattice-mismatched strain also changes the subband dispersions in the absence of magnetic fields.[20,21] This results in the modification of the Landau level structures.

In Fig. 2, we show the Landau level structures for the InAs/GaSb quantum wells with a 15-nm InAs layer and a 5-nm GaSb layer under flatband conditions. Panel (a) is for the quantum well structure grown on the InAs substrate, while panel (b) is for that grown on the GaSb substrate. The InAs conduction band edge in the absence of strain is taken as the energy reference. Levels of three subbands resulting from spatial quantization are shown in each panel of Fig. 2. The states of these subbands at zero magnetic field are labeled as 1hh and 2hh for the first and second heavy-hole subbands and $1e$ for the first electron subband. The electron level at $B=0$ is lower than the 1hh level in each panel of Fig 2. At nonzero magnetic fields each level splits into a number of levels due to the formation of Landau levels and the Zeeman effect, which is responsible for the spin splitting. We show the electron and hole Landau levels for four quantum numbers: $n=-2$, -1, 0, and 1, which are indicated in Fig. 2. For $n=-2$, only one 1hh level and one 2hh level with a Landau level index $\nu=0$ and spin $s=-1/2$ exist in each of the considered quantum well structures. For $n=-1$, we have a 1hh level and a 2hh level with $\nu=1$ and spins opposite to the magnetic field direction. There also exists a $1e$ level with spin $s\approx -1/2$ and $\nu=0$. For $n=0$, there are two $1e$ levels of $\nu=0$ and 1 with spins along and opposite to the magnetic field and heavy-hole states of index $\nu=2$ and $s\approx -1/2$. For $n=1$, we have two $1e$ states of $\nu=1$ and 2 with opposite spins and heavy-hole states of $\nu=0$ with $s\approx 1/2$ and $\nu=3$ with $s\approx -1/2$.

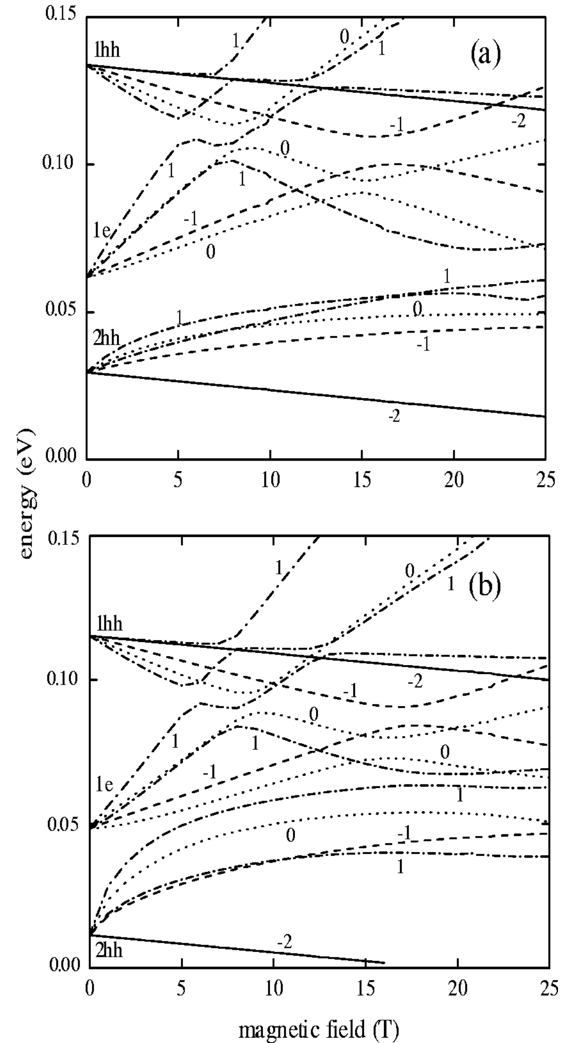

FIG. 2. Landau level structures for the AlSb/InAs/GaSb/AlSb quantum well with a 15-nm InAs layer and a 5-nm GaSb layer grown on (a) the InAs substrate and (b) the GaSb substrate at zero electric field.

With the magnetic field increasing, the electron levels move upward while the 1hh levels move downward. The 2hh level of index $\nu=0$ with spin $s=-1/2$ moves downward while the other 2hh levels move upward. This difference can be explained by the mixing of the heavy-hole states with the electron (light-hole) states for nonzero magnetic fields. The 2hh state of index $\nu=0$ and $s=-1/2$ does not mix with other states so that its behavior is typical for the hole states. At some nonzero magnetic fields the $1e$ levels anticross with the 1hh levels of the same quantum number n. This produces gaps in the Landau level structures of the wells both grown on InAs and on GaSb. As shown in Fig. 2, different strain conditions [in panel (a) the GaSb layer is strained while in panel (b) the InAs layer is strained] result in different Landau level positions. Comparing the results presented in panel (a) and panel (b), we can conclude that the neglect of lattice-mismatched strain can produce an error of the order of 10 meV in Landau level positions. It should be noted that the band-bending caused by charge accumulation in the quantum wells can also produce the shifts in the energy level positions. Such shifts are of the order of 10 meV in the absence of magnetic fields[5,19] for the structures where the electron and hole charges result only from the carrier transfer through the InAs/GaSb interface. However, they can be considerably reduced in realistic structures with the donor and acceptor impurities or defects, whose charges compensate the negative electron charge in InAs and the positive hole charge in GaSb.

Let us consider the lowest electron-like levels before and after anticrossings in Figs. 2(a) and 2(b). The $1e$ state of $\nu=0$ and spin along the magnetic field is the lowest state before the anticrossing in each panel. It anticrosses with the 1hh-like state of $\nu=2$ and spin $s\approx-1/2$, which in turn anticrosses at lower magnetic fields with the $1e$ state of $\nu=1$ and spin $s\approx-1/2$. The latter state eventually becomes the lowest electronlike state of $\nu=0$ and $s\approx1/2$ after two anticrossings. The $1e$ state of $\nu=0$ and $s\approx-1/2$ is the second lowest state at low magnetic fields in each panel of Fig. 2. It is slightly higher than the corresponding state with $s\approx1/2$. This state anticrosses with the 1hh state of $\nu=1$ and spin $s\approx-1/2$ which become the electronlike $\nu=0$ and $s=-1/2$ after anticrossing in each figure. It can be clearly seen that the spin splitting between the states of the Landau level index $\nu=0$ is more significant in Fig. 2(b) than in Fig. 2(a) before anticrossings and vice versa after anticrossings. The spin splitting of the next Landau levels of $\nu=1$ is negligible at low magnetic fields, but becomes noticeable at higher magnetic fields after the anticrossings. It is greater for the structure grown on InAs than for the structure grown on GaSb. It should be noted that the spin splitting of the hole levels of index $\nu=0$ after the anticrossings with the electronlike states is greater in panel (b) than in panel (a). Contrary to the results presented in Ref. 15 for a similar structure, it is much less than the spin splitting of the electron levels of the same Landau level index. Also, unlike Ref. 15, the latter considerably enlarges after anticrossings with the hole states.

A positive voltage bias applied across the InAs/GaSb quantum well causes shifts in the positions of the electronlike and the heavy-hole-like energy levels. As a result, the separation between the $1e$ level and the 1hh level at zero magnetic field decreases. This can be clearly seen from Fig. 3, where we show the Landau levels of the quantum well structures identical to those for Fig. 2 except under an electric field $|\mathcal{E}|=25$ kV/cm. Similarly, panel (a) in this figure is for the structure grown on InAs and panel (b) is for the structure grown on GaSb. We suppose that the reference zero energy is at the conduction band edge of the left boundary (at $z=0$, see Fig. 1) of the InAs layer. Since at zero bias the highest heavy-hole-like Landau level is above the lowest electronlike Landau level at magnetic fields up to 25 T (see Fig. 2), the electron-hole system in such situations is in a semimetal phase at sufficiently high magnetic fields, where electrons in the InAs layer can coexist with holes in the GaSb layer. This means that the critical magnetic field B_c, at which the SSPT occurs, is higher than 25 T at $\mathcal{E}=0$. The critical magnetic field decreases with the voltage increasing. It reduces approximately to 20 T for the structure grown on InAs for $|\mathcal{E}|=25$ kV/cm, and approximately to 21.5 T for the structure grown on GaSb under the same bias voltage. At

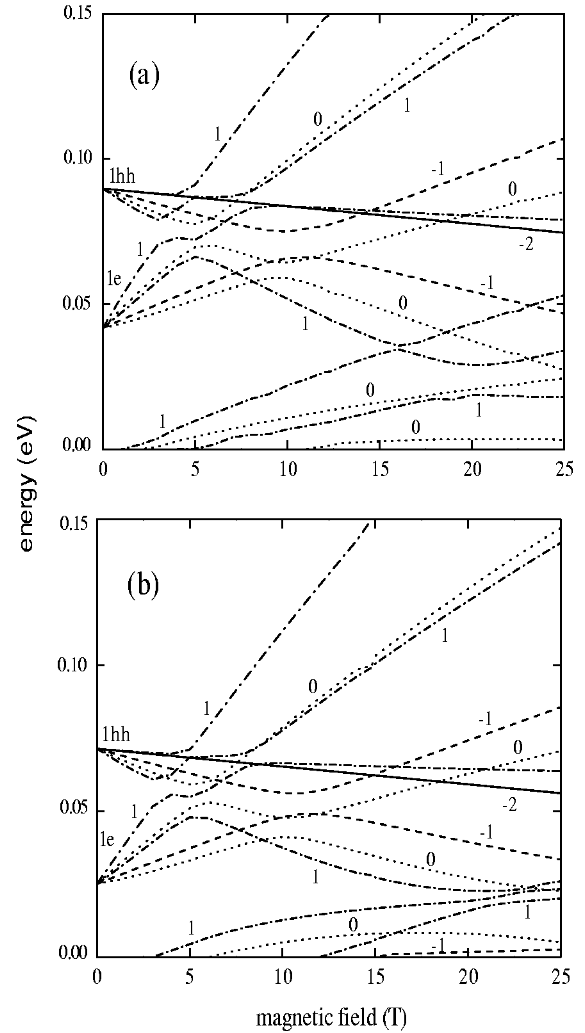

FIG. 3. Landau level structures for the AlSb/InAs/GaSb/AlSb quantum well with a 15-nm InAs layer and a 5-nm GaSb layer grown on (a) the InAs substrate and (b) the GaSb substrate at the electric field $|\mathcal{E}|=25$ kV/cm.

$|\mathcal{E}|=35$ kV/cm, B_c decreases approximately to 15.5 T for the structure grown on InAs and approximately to 16.5 T for the quantum well grown on GaSb, as our calculations show. For $B>B_c$, the highest heavy-hole-like level is below the lowest electronlike level and accordingly, the system is in a semiconducting phase. As the Landau level structures show, for a sufficiently high magnetic field, the semimetal phase at $\mathcal{E}=0$ can change to a semiconducting phase with the normal electric field increasing. A phase transition can also occur at a given electric field but with the magnetic field increasing, as can be seen from Fig. 3. Note that, in the structures with thick AlSb barriers only a small fraction of the total bias drops across the InAs and GaSb layers, which decreases with the increase of carrier concentrations in the well due to the screening of external electric field. This results in less pronounced shifts of the electron and hole levels towards each other with the external electric field.[29] On the other hand, the negative electron charge in InAs and the positive hole charge in GaSb produce the band-bendings which reduce the separation between the 1hh and $1e$ levels at zero bias.[5,19] A self-consistent calculation is required to clarify the resultant influence of these two effects on level positions and B_c.

Finally, in Fig. 4 we present the results for the effective g factors calculated for the lowest electron and the highest hole states of Landau level index $\nu=0$. We define $g=\Delta E/(\mu_B B)$, where ΔE is the energy separation between the spin-up and spin-down electronlike (holelike) states and μ_B is the Bohr magneton. Note that both the Zeeman effect and the Rashba effect contribute to the so-defined g factors. Panels (a) and (b) in Fig. 4 correspond to $\mathcal{E}=0$ and $|\mathcal{E}|=25$ kV/cm, respectively. Curves 1 and 2 in each panel reflect the variations of the heavy-hole effective g-factors with the magnetic field for the quantum well structures grown on InAs and GaSb, respectively. The variations of the corresponding electron effective g-factors are represented by curves 3 and 4. This is interesting that the hole effective g factor oscillates with the magnetic field because of multiple anticrossings of electron and hole levels. Also, it changes the sign several times. The positions of maxima and minima of the hole g factor shift to lower magnetic fields with the applied bias increasing, because of the changes in the positions of the electron-hole level anticrossings. The effective g factor of holes at high magnetic fields is positive and does not depend essentially on the voltage across the quantum well. Its value is greater for the structure grown on GaSb than for the structure grown on InAs. The effective g factor of electrons is always negative as in a bulk InAs and its absolute value has the maxima at $B\approx 0$ and at the point of the anticrossing with the hole states. Since the positions of the anticrossings vary with the bias, the effective g factor also depends on the bias. The difference between the electron effective g factors in structures grown on InAs and on GaSb can be as large as 10 at low magnetic fields for $\mathcal{E}=0$, but it becomes very small for $|\mathcal{E}|=25$ kV/cm, as can be seen in Fig. 4.

The variations in the Landau level positions and in the spin splitting of the Landau levels in structures with different strains can be detected in cyclotron resonance and magnetotransport measurements.[2,8,9,16,17,26,27] The spin-splitting results in additional regions of zero magnetoresistance, the positions of which depend on the lattice-mismatched strain and the applied voltage. The values of critical magnetic field B_c for structures under different growth conditions can be found by reducing to zero of carrier (hole) concentration with increasing B. However, so-obtained values of B_c are less than those at which the lowest electron level crosses the highest hole level when the excess of electrons exists.[8,12,16,26,27] The effect of lattice-mismatched strain on the spin splitting of levels and critical magnetic fields, to our best knowledge, has not yet been investigated experimentally, although some detailed investigations of the dependence of B_c on the structure parameters for InAs/$Al_xGa_{1-x}Sb$ quantum wells and InAs/GaSb superlattices at zero bias were carried out in Refs. 8 and 9. The obtained values $B_c\approx 40$ T for structures with layers of different thicknesses[9] are in a satisfactory agreement

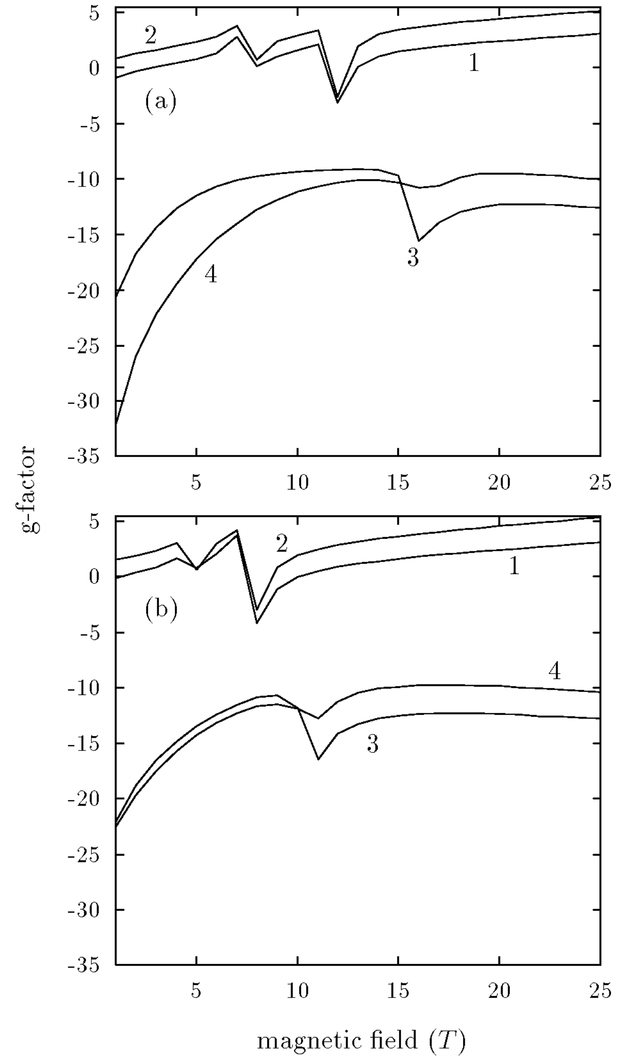

FIG. 4. Dependencies of the electron and hole effective g factors in the AlSb/InAs/GaSb/AlSb quantum wells on the magnetic field at (a) zero electric field and (b) the electric field $|\mathcal{E}|=25$ kV/cm. Curves 1 and 2 in each panel are for the effective g factors of heavy holes in the structures grown on InAs and GaSb, respectively. Curves 3 and 4 are for the effective g factors of electrons in the structures grown on InAs and GaSb, respectively.

with the value found here (about 30 T). Some discrepancy can be due to the heavy-hole effective mass anisotropy in the plane of the structure neglected in the present work. The values of B_c for InAs/Al_xGa_{1-x}Sb quantum wells with the 15-nm InAs layer[8] for $x=0.2$ and 0.1 ($B_c=5$ and 14 T, respectively) are also in agreement with our predictions taking into account the dependence of B_c on x. The investigation of InAs/GaSb quantum wells both under magnetic and electric fields,[12,16,26,27] showed a decrease of B_c to 4 T for the structure with 30-nm InAs and 15-nm GaSb layers separated by a 5-nm AlSb layer at the external electric field $|\mathcal{E}| \approx 140$ kV/cm,[16] which was considerably screened by carriers in the well. (Our model gives $B_c=4$ T at $|\mathcal{E}|\sim 80$ kV/cm for the parameters described above.) On the other hand, the hole concentration was found negligibly small at the positive voltages across the thinner layer structure,[12,26] because of very high electron concentrations.

In summary, we have applied the scattering matrix method and Burt's envelope function theory for investigation of the electronic band structures of InAs/GaSb quantum wells under the magnetic and the electric fields perpendicular to the interfaces. The quantum well structures grown on InAs and GaSb have been investigated taking into account the lattice-mismatched strain. The Landau level positions and the spin splitting of Landau levels are found to be sensitive to the lattice-mismatched strain and the applied voltage. We have found that the spin splitting of the lowest electron levels is larger for the structure grown on InAs than that for the structure grown on GaSb at high magnetic fields. The spin splitting of the highest hole levels of index $\nu=0$ is greater for the structure grown on GaSb than for the structure grown on InAs and is much less than that of the electron levels at high magnetic fields in the model used. We have shown that the positive voltage bias across the InAs/GaSb quantum well can reduce the critical magnetic field B_c of the SSPT. The critical field B_c is slightly higher for the structure grown on GaSb than grown on InAs. We have also found that for a given magnetic field the SSPT can be conditioned by the positive bias across the InAs/GaSb quantum wells.

ACKNOWLEDGMENTS

The authors would like to thank Yoshiro Hirayama and Kyoichi Suzuki for stimulating discussions of their experimental data. This work was financially supported by the Russian Foundation for Basic Research under Grant No. 03-02-16788.

APPENDIX

In accordance with Eq. (8), the envelope function $\mathbf{F}$ in the lth layer can be written as

$$\mathbf{F}=\exp(ik_y y)\sum_{j=1}^{m}\,[a_j^{(l)}\exp[ik_{z,j}^{(l)}(z-z_{l-1})]\mathbf{h}_{+j}^{(l)}+b_j^{(l)} \times\exp[-ik_{z,j}^{(l)}(z-z_l)]\mathbf{h}_{-j}^{(l)}], \tag{A1}$$

where $m=4$ for $n\geqslant 1$, $m=3$, 2, and 1 for $n=0$, -1, and -2, and z_{l-1} and z_l are the z coordinates of the left and right boundaries of the lth layer. The coefficients $a_j^{(l)}$ and $b_j^{(l)}$, respectively, are for the forward and the backward waves in the lth layer. The vector functions $\mathbf{h}_{\pm j}^{(l)}$ for the forward and the backward waves are defined as

$$[e_{\pm j1}f_n(x')e_{\pm j2}f_{n-1}(x')e_{\pm j3}f_{n+1}(x')e_{\pm j4}f_{n+2}(x')]^T,$$

and the vectors $\mathbf{e}_{\pm j}$ are obtained from the corresponding vectors $\mathbf{C}$ in Eq. (8) by deleting C_1 and C_4. We set $e_{\pm jk}=0$, if the corresponding harmonic oscillator function is zero. Then the coefficients for two neighboring layers can be connected by a transfer matrix

$$M^{(l+1)}=\begin{pmatrix} D^{(l)-1} & 0 \\ 0 & I \end{pmatrix}\bar{M}^{(l+1)}\begin{pmatrix} I & 0 \\ 0 & D^{(l+1)} \end{pmatrix} \tag{A2}$$

as

$$\begin{pmatrix} \mathbf{a}^{(l)} \\ \mathbf{b}^{(l)} \end{pmatrix}=M^{(l+1)}\begin{pmatrix} \mathbf{a}^{(l+1)} \\ \mathbf{b}^{(l+1)} \end{pmatrix}, \tag{A3}$$

where I is the $m\times m$ identity matrix, and $D^{(l)}$ is an $m\times m$ diagonal matrix with the elements $D_{ij}^{(l)}=\delta_{ij}\exp[ik_{z,j}^{(l)}(z_l-z_{l-1})]$. The $(2m)\times(2m)$ nonsingular matrix $\bar{M}^{(l+1)}$ can be expressed as

$$\bar{M}^{(l+1)}=\begin{pmatrix} \mathbf{e}_+^{(l)} & \mathbf{e}_-^{(l)} \\ \mathbf{f}_+^{(l)} & \mathbf{f}_-^{(l)} \end{pmatrix}^{-1}\begin{pmatrix} \mathbf{e}_+^{(l+1)} & \mathbf{e}_-^{(l+1)} \\ \mathbf{f}_+^{(l+1)} & \mathbf{f}_-^{(l+1)} \end{pmatrix}, \tag{A4}$$

where for $m=4$, $\mathbf{e}_\pm^{(l)}=(\mathbf{e}_{\pm 1}^{(l)}\ \mathbf{e}_{\pm 2}^{(l)}\ \mathbf{e}_{\pm 3}^{(l)}\ \mathbf{e}_{\pm 4}^{(l)})$ and $\mathbf{f}_\pm^{(l)}=(\mathbf{f}_{\pm 1}^{(l)}\ \mathbf{f}_{\pm 2}^{(l)}\ \mathbf{f}_{\pm 3}^{(l)}\ \mathbf{f}_{\pm 4}^{(l)})$, $\mathbf{f}_{\pm j}^{(l)}=\hat{H}_B\mathbf{e}_{\pm j}^{(l)}$. In operator $\hat{H}_B$, $\hat{k}_z$ is replaced by $\pm k_{z,j}^{(l)}$ for the forward and the backward waves, respectively, the operator $\hat{K}_+$ is replaced by $\sqrt{q/2}$, and the operator $\hat{K}_-$ in TB_-, CB_-, and SB_- is replaced by $2(n+1)\sqrt{q/2}$, $2n\sqrt{q/2}$, and $2(n+2)\sqrt{q/2}$, respectively in accordance with the definition of $f_n(x')$ in Sec. III. However, operators are replaced by zero, if they are applied to a harmonic oscillator function equal to zero. For $m=3$, 2, and 1 the matrices $\mathbf{e}_\pm^{(l)}$, and $\mathbf{f}_\pm^{(l)}$ are formed by 3, 2, and 1 vectors $\mathbf{e}_{\pm j}^{(l)}$ and $\mathbf{f}_{\pm j}^{(l)}$ with zero components removed. In this way we obtain the 8×8, 6×6, 4×4, and 2×2 transfer matrices for quantum numbers $n\geqslant 1$, $n=0$, $n=-1$, and $n=-2$, respectively. These matrices depend on the lattice-mismatched strain because the strain influences both the bulk solutions in each layer and the boundary conditions. Using the obtained transfer matrices, we calculate, as in Refs. 24 and 25, the scattering matrices $S(l,k)$, defined as

$$\begin{pmatrix} \mathbf{a}^{(k)} \\ \mathbf{b}^{(l)} \end{pmatrix}=S(l,k)\begin{pmatrix} \mathbf{a}^{(l)} \\ \mathbf{b}^{(k)} \end{pmatrix}. \tag{A5}$$

In Eq. (A5) indices l and k correspond to the lth and kth layers. The dispersions in the quantum well are then solved using the equation[25]

$$|I-S_{21}(l,N)S_{12}(1,l)|=0, \tag{A6}$$

where the left barrier layer is the first layer and the right barrier layer is the Nth layer, $1<l<N$, $S_{ij}(l,k)$ is the $m\times m$ submatrix of the corresponding scattering matrix.

[1] G.A. Sai-Halasz, L. Esaki, and W.A. Harrison, Phys. Rev. B **18**, 2812 (1978).
[2] Y. Guldner, J.P. Vieren, P. Voisin, M. Voos, L.L. Chang, and L. Esaki, Phys. Rev. Lett. **45**, 1719 (1980).
[3] S.R. White and L.J. Sham, Phys. Rev. Lett. **47**, 879 (1981).
[4] G. Bastard, E.E. Mendez, L.L. Chang, and L. Esaki, J. Vac. Sci. Technol. **21**, 531 (1982).
[5] M. Altarelli, Phys. Rev. B **28**, 842 (1983).
[6] A. Fasolino and M. Altarelli, Surf. Sci. **142**, 322 (1984).
[7] G. Grosso, S. Moroni, and G.P. Parravicini, Phys. Rev. B **40**, 12328 (1989).
[8] I. Lo, W.C. Mitchel, and J.-P. Cheng, Phys. Rev. B **48**, 9118 (1993).
[9] D.J. Barnes, R.J. Nicholas, R.J. Warburton, N.J. Mason, P.J. Walker, and N. Miura, Phys. Rev. B **49**, 10474 (1994).
[10] D.M. Symons, M. Lakrimi, R.J. Warburton, R.J. Nicholas, N.J. Mason, P.J. Walker, M.I. Eremets, and G. Hill, Phys. Rev. B **49**, 16614 (1994).
[11] J.J. Quinn and J.J. Quinn, Surf. Sci. **361**, 930 (1996).
[12] M.J. Yang, C.H. Yang, B.R. Bennett, and B.V. Shanabrook, Phys. Rev. Lett. **78**, 4613 (1997).
[13] M. Lakrimi, S. Khym, R.J. Nicholas, D.M. Symons, F.M. Peeters, N.J. Mason, and P.J. Walker, Phys. Rev. Lett. **79**, 3034 (1997).
[14] A.R. Rundell, G.P. Srivastava, and J.C. Inkson, Phys. Rev. B **55**, 5177 (1997).
[15] S.-F. Tsay, J.-C. Chiang, Z.M. Chau, and I. Lo, Phys. Rev. B **56**, 13 242 (1997).
[16] L.J. Cooper, N.K. Patel, V. Drouot, E.H. Linfield, D.A. Ritchie, and M. Pepper, Phys. Rev. B **57**, 11 915 (1998).
[17] S.K. Singh, B.D. McCombe, J. Kono, S.J. Allen, Jr., I. Lo, W.C. Mitchel, and C.E. Stutz, Phys. Rev. B **58**, 7286 (1998).
[18] A.J.L. Poulter, M. Lakrimi, R.J. Nicholas, N.J. Mason, and P.J. Walker, Phys. Rev. B **60**, 1884 (1999).
[19] S. de-Leon, L.D. Shvartsman, and B. Laikhtman, Phys. Rev. B **60**, 1861 (1999).
[20] R. Magri, L.W. Wang, A. Zunger, I. Vurgaftman, and J.R. Meyer, Phys. Rev. B **61**, 10 235 (2000).
[21] A. Zakharova, S.T. Yen, and K.A. Chao, Phys. Rev. B **66**, 085312 (2002).
[22] M.G. Burt, J. Phys.: Condens. Matter **4**, 6651 (1992).
[23] B.A. Foreman, Phys. Rev. B **56**, R12748 (1997).
[24] D.Y.K. Ko and J.C. Inkson, Phys. Rev. B **38**, 9945 (1988).
[25] A. Zakharova, S.T. Yen, and K.A. Chao, Phys. Rev. B **64**, 235332 (2001).
[26] M.J. Yang, C.H. Yang, and B.R. Bennett, Phys. Rev. B **60**, R13958 (1999).
[27] T.P. Marlow, L.J. Cooper, D.D. Arnone, N.K. Patel, D.M. Whittaker, E.H. Linfield, D.A. Ritchie, and M. Pepper, Phys. Rev. Lett. **82**, 2362 (1999).
[28] M. Altarelli, J.C. Maan, L.L. Chang, and L. Esaki, Phys. Rev. B **35**, 9867 (1987).
[29] Y. Naveh and B. Laikhtman, Appl. Phys. Lett. **66**, 1980 (1995).
[30] E. Halvorsen, Y. Galperin, and K.A. Chao, Phys. Rev. B **61**, 16 743 (2000).
[31] R. Magri and A. Zunger, Phys. Rev. B **65**, 165302 (2002).
[32] G.L. Bir and G.E. Pikus, *Symmetry and Strain-Induced Effects in Semiconductors* (Wiley, New-York, 1974).
[33] A. Zakharova and K.A. Chao, J. Phys.: Condens. Matter **14**, 5003 (2002).
[34] C.Y.-P. Chao and S.L. Chuang, Phys. Rev. B **46**, 4110 (1992).
[35] T.B. Bahder, Phys. Rev. B **41**, 11992 (1990); **46**, 9913 (1992).
[36] T.B. Bahder, Phys. Rev. B **45**, 1629 (1992).
[37] M.P.C.M. Krijn, Semicond. Sci. Technol. **6**, 27 (1991).